NUMERICAL AND OPTICAL ANALYSIS OF WEATHER ADAPTABLE SOLAR REACTOR

Usman S. and Ozalp N.*
*Author for correspondence
Texas A&M University at Qatar,
Mechanical Engineering Department,
P.O. Box 23874 Doha, Qatar, nesrin.ozalp@qatar.tamu.edu

ABSTRACT

Solar energy is an abundant renewable energy resource that can be used to provide high process heat necessary to run thermo chemical processes for production of various solar fuels and commodities. In a solar reactor, sunlight is concentrated into a receiver through a small opening called the aperture. However, obtaining and maintaining semi-constant high temperatures inside a solar reactor is a challenge. This is because the incident solar radiation can fluctuate depending on the position of the sun and the weather conditions. For fixed aperture size reactors, changes in incident solar flux directly affect the temperature inside the reactor. This paper presents a novel solar reactor with variable aperture mechanism which is designed and manufactured at our lab. Radiation heat transfer analysis of this reactor concept is studied via Monte Carlo (MC) ray tracing. MC ray tracing module is coupled to a steady state one-dimensional energy equation solver. Energy equation is solved for the wall and gas, accounting for the absorption, emission, and convection. Incoming direct flux values for a typical day are obtained from National Renewable Energy Lab (NREL) database. Results show that for a perfectly insulated reactor, the average temperature of the working fluid may be kept appreciably constant throughout the day if aperture diameter is varied between 3 cm and 1.5 cm for incoming fluxes starting with 400 W/m^2 at 05:12 am in the morning, reaching peak value of 981 W/m^2 at noon, and eventually receiving 400 W/m^2 at 6:58pm in the evening, which can make the solar reactor run about 13 hours continuously at 1500K semi-constant temperature.

INTRODUCTION

The earth and its atmosphere receive solar energy at the rate of approximately *1.7 X 10^{17} W* [1]. Radiation from the sun reaching the earth's surface has low flux density of the order of a few hundred Watts per square meter. However, once concentrated, it can be used to provide high temperature process heat necessary for electricity production via solar thermal [2] or for solar thermochemical processing to produce metals [3], syngas [4, 5] or hydrogen [6-8]. Such high temperature processes require maintaining a semi-constant temperature for stable efficiency. However, the incoming solar energy is inherently transient due to varying position of the sun and changing weather conditions leading to fluctuations in the available flux density. This makes it difficult to maintain a constant temperature resulting in lower process efficiency. Therefore, it is important to design a system that can solve this problem by maintaining semi-constant temperatures for these processes so that the production rate is kept high irrespective of fluctuations in solar energy.

Regardless of the process, the basic principle involved is the collection of solar energy over a large area using reflectors and directing it towards a high temperature resistant receiver through a small opening called the aperture. In case of thermochemical processing, the cavity receiver absorbs the concentrated solar energy coming through the aperture and transfers it to the working fluid entraining the reactants. There have been many such remarkable solar reactor designs for various thermochemical processes [9-12]. An important point to be noted is that all these solar reactor concepts employ a fixed aperture size, which does not compensate for fluctuations in incoming solar energy.

To address the problem of low production efficiency because of intermittent solar energy, we developed a novel concept for a variable size aperture inspired by the human eye, where pupils enlarge in the dark and shrink when exposed to light. The objective of this work is to investigate the efficacy of variable size apertures in maintaining a semi-constant temperature in the reactor irrespective of fluctuations in incoming solar flux. This paper presents an optical and heat transfer analysis of our prototype reactor concept with variable size aperture exposed to changing solar flux.

METHODOLOGY

The prototype reactor used for the analysis is shown in Figure 1. It has three inlet ports through which the working fluid enters and a single exit port through which it leaves the reactor. The inlet ports are positioned such that a vortex flow is formed inside the reactor. The front plate has an opening called the aperture whose size can be varied to control the amount of incoming solar energy. In order to house the reactants inside the reactor and allow incoming radiation from the aperture into the receiver, a quartz window is fitted right behind the aperture.

The reactor is positioned such that the aperture is in the focal plane of the solar concentrator.
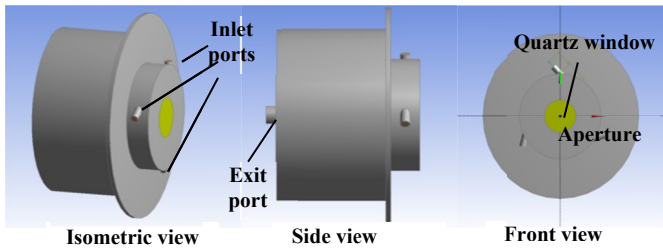

Figure 1 Prototype reactor geometry

For the optical analysis presented in this paper solar furnace configuration of Paul Scherrer Institute (PSI) is used [13]. This high-flux solar furnace is capable of delivering a peak concentration ratio, C_{peak} of approximately 5530 suns (1 sun = 1kW/m^2) with a distribution that is approximately Gaussian, where the mean concentration ratio, $\bar{C}$ is defined as the ratio between power intercepted by the aperture (P_{ap}) and the direct normal insolation (I) at the aperture. Due to the Gaussian distribution, the mean concentration ratio varies as a function of aperture diameter (D_{ap}) and is given by $\bar{C}(D_{ap}) = \frac{P_{ap}}{I \pi (\frac{D_{ap}^2}{4})}$.

Figure 2 shows mean concentration ratios $\bar{C}(D_{ap})$ from experimental results given in [13] for different aperture diameters.
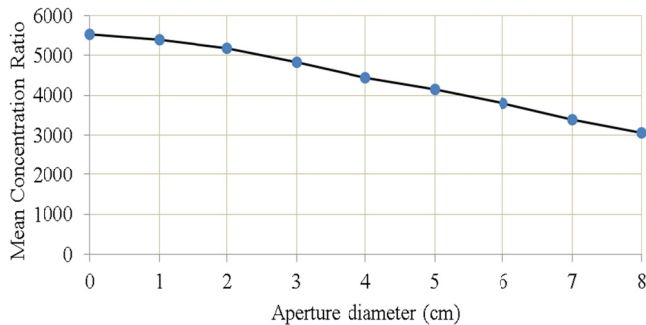

Figure 2 Mean concentration ratio through a circular aperture as a function of its diameter.

In present study, a typical daily cycle of direct normal radiation (I) from the sun is obtained from the National Renewable Energy Laboratory (NREL) database [14]. The calculated normal insolation is based on clear sky model by Bird et. al. [15]. This corresponds to clear sky conditions on July 1, 2011, at the Solar Radiation Research Laboratory (SRRL) of NREL located at latitude *39.4^o N*, longitude *105.18^o W* at an altitude of *1829 m* above mean sea-level.

Figure 3 shows the normal beam insolation for the entire day as position of the sun changes and the direct irradiance reaches a peak of approximately 981 W/m^2 at 1231 hrs. Using mean concentration ratio of the paraboloidal concentrator and the normal beam insolation we can calculate the power intercepted by the aperture (P_{ap}) as a function of its diameter. Figure 4

shows P_{ap} $(= \frac{\bar{C}(D_{ap}) \pi D_{ap}^2 I}{4})$ calculated as a function of aperture diameter for beam normal radiation (I) equal to 200 W/m^2 (at 0449 hrs and 1921 hrs), 400 W/m^2 (at 0512 hrs and 1858 hrs), 600 W/m^2 (at 0544 hrs and 1826 hrs), 800 W/m^2 (at 0650 hrs and 1719 hrs) and 981 W/m^2 (at 1231 hrs).
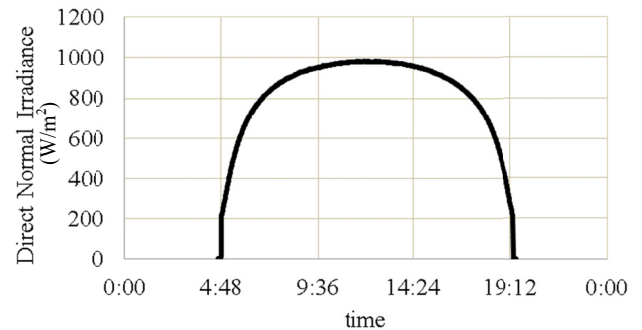

Figure 3 Bird estimated direct normal insolation (I).

An aperture size of 4 cm intercepts a maximum of about 5.5 kW for a peak normal beam insolation of 981 W/m^2 at 1231 hrs. For the same aperture size, this reduces to 1.12 kW for normal insolation of 200 W/m^2 in the morning at 0449 hrs and evening at 1921 hrs. We see that there is a 5 times decrease in the total intercepted power at the aperture between noon and the morning or evening. Therefore, in order to maintain a semi-constant temperature inside the reactor, it is necessary to use variable size apertures. For a particular time of the day, depending on the magnitude of direct normal insolation, there exists an optimum aperture size that can maintain the desired level of temperature inside the reactor. For the same amount of insolation, larger aperture size implies higher P_{ap}, but this may not necessarily mean higher temperature. This is because a larger aperture size may cause higher re-radiation losses back through the aperture. This would lead to a drop in cavity receiver temperatures. For a smaller aperture, though P_{ap} is less, re-radiation losses may be lower. Thus, selecting an optimum aperture size for a particular time of the day is a compromise between maximizing radiation capture and minimizing re-radiation losses [16].
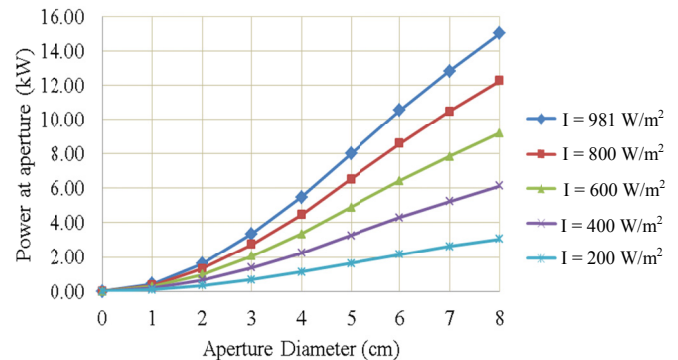

Figure 4 Power intercepted at aperture (P_{ap}) as a function of diameter for different levels of normal insolation.

The incoming solar radiation intercepted at the aperture undergoes absorption and reflection at the receiver walls. Some of the reflected rays are further reflected or absorbed by the walls. Some escape back through the aperture as re-radiation. The power absorbed by the walls is then transferred to the working fluid by convection. Maintaining a semi-constant gas temperature inside the reactor thus necessitates a detailed know how of the heat transfer mechanisms inside the reactor. Keeping this objective in mind, we have modeled the heat transfer characteristics of a prototype reactor manufactured in our lab. A one-dimensional steady state heat transfer model is developed which is coupled to the Monte Carlo ray tracing technique [17, 18] to calculate radiative heat exchange in the reactor.

Heat Transfer Analysis

For heat transfer analysis we have used a simplified cross-section of the prototype as shown in Figure 5. The reactor consists of two cylindrical cavities, designated as c_1 and c_2. The cylindrical cavity c_1 has a length, inner radius and outer radius of $L_1 = 39.7$ mm, $R_{1in} = 40$ mm and $R_{1out} = 65$ mm respectively. The cavity c_2 has length, inner radius and outer radius of $L_2 = 135$ mm, $R_{2in} = 76.2$ mm, and $R_{2out} = 91.2$ mm respectively. The cylindrical cavities c_1 and c_2 are connected via a circular plate cp in the form of a ring of inner radius $Rcp_{in} = R_{1in}$ and outer radius of $Rcp_{out} = R_{2in}$. The plate has thickness $t_{cp} = 5$ mm. The cavity c_1 has three inlet ports that inject the working fluid into the reactor as shown in Figure 1. It is attached to a front plate fp which has a quartz window that receives radiation through a circular aperture of radius R_{ap} mounted in front of it. The reactor is positioned such that the aperture is in the focal plane of solar concentrator. The front plate is a ring of thickness $t_{fp} = 5$ mm, inner radius equal to the radius of the aperture, R_{ap} and outer radius, $Rfp_{out} = R_{1in}$. The cylindrical cavity c_2 has a back plate bp of thickness $t_{bp} = 10$ mm and outer radius of $Rbp_{out} = R_{2in}$. It has an exit port of radius $R_{ex} = 8.5$ mm through which the working fluid exits the reactor. A co-ordinate system is positioned at the aperture such that z-axis lies along the axis of the cylindrical cavities as shown in Figure 5.
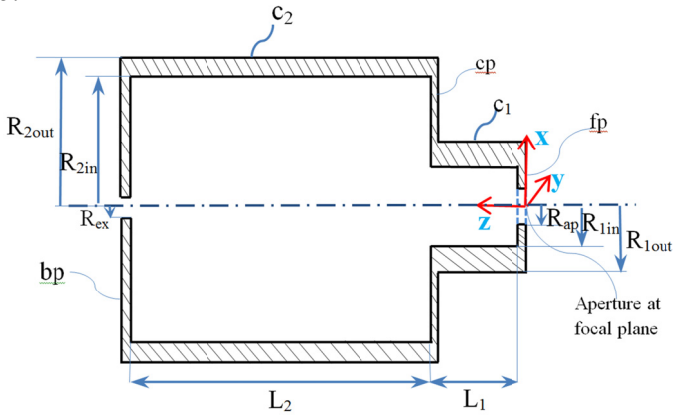

Figure 5 Simplified schematic of cross-section of prototype reactor

For the numerical model developed here, all exterior surfaces of the reactor are assumed to be perfectly insulated. The interior surfaces of the cavity are assumed to be diffuse-gray and the quartz window is assumed to be a perfectly transmitting material. The working fluid air is modelled as a non-participating medium [17]. For simplifying the analysis, radiation properties are assumed to be independent of temperature.

For heat transfer analysis of the reactor, steady state conservation of energy is applied to the subsystems, namely, cylindrical cavity c_1, cylindrical cavity c_2, front plate fp, connecting plate cp, back plate bp and the working fluid g (air). The objective here is to obtain the variation of temperature of the cavity walls and gas flow in z-direction. Considering this, the reactor walls and fluid domain is split into different control volumes, and analysis is done by solving the steady state energy equations for each such volume.

First consider the cavity c_1. It is split into $M1$ isothermal ring elements of equal widths, $w_{c1} = L_1/M1$, with inner and outer radius given by R_{1in} and R_{1out}. Here, we neglect axial conduction and assume that outer surface is perfectly insulated. A representative control volume with all incoming and outgoing energy is indicated in Figure 6. The element, i is irradiated by solar radiation and by radiation emitted by other volume elements - of cavities c_1 and c_2, front plate (fp), connecting plate (cp) and back plate (bp). A part of it is absorbed $(Q_{ab,c1,i} = Q_{1,ab,c1,i} + Q_{2,ab,c1,i})$ and the rest is transferred to the adjacent gas phase via convection $(Q_{conv,c1-g,i})$ or re-radiated as emitted energy $(Q_{em,c1,i})$.
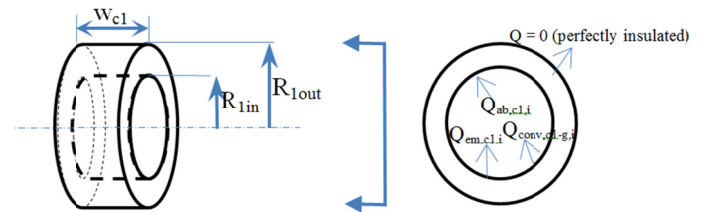
Figure 6 On the left is a representative control volume from cavity c_1. Incoming and outgoing energy to this element is shown on the right (for a front view of the control volume).

Assuming steady state heat transfer, the first law of thermodynamics (energy conservation) for the ith cavity wall ring element can be written as,

$$Q_{ab,c1,i} - Q_{em,c1,i} - Q_{conv,c1-g,i} = 0 \qquad (1)$$

The absorption term, $Q_{ab,c1,i}$ is composed of two components. $Q_{1,ab,c1,i}$ is from incident solar radiation coming from the aperture while $Q_{2,ab,c1,i}$ is due to emissions from other reactor wall elements of c_1, c_2, fp, cp and bp. The contribution of absorption terms are unknown and are found using the Monte Carlo ray tracing method explained later. The emission term is given by,

$$Q_{em,c1,i} = A_{c1}\,\varepsilon\,\sigma\,T_{c1,i}^4 \tag{2}$$

For all interior surfaces of the reactor, the total hemispherical emissivity is taken as, $\varepsilon = 0.8$ [19] and σ is the Stefan-Boltzmann constant given by $5.67\times10^{-8}\ W\ m^{-2}\ K^{-4}$. The area $A_{c1} = 2\pi R_{1in}\ w_{c1}$. The convection term is given by,

$$Q_{conv,c1-g,i} = h_{c1-g}\,A_{c1}\,(T_{c1,i} - T_{g,i}) \tag{3}$$

The heat transfer coefficient h_{c1-g} is calculated from heat transfer correlation for Nu given in [19, 20],

$$Nu = 0.042\,Re^{0.8} \tag{4}$$

The Reynolds number, Re is taken as 3491 as given by fluid dynamic simulations in [19]. Once Nu is obtained it can be plugged in to equation (5) to obtain h_{c1-g}.

$$Nu = \frac{h_{c1-g}\,D_{c1}}{k_g} \tag{5}$$

D_{c1} is the inner diameter of cavity c_1. The thermal conductivity of air, k_g is calculated a function of the average gas temperature. Substituting equations (2) and (3) in (1) we obtain,

$$Q_{ab,c1,i} - A_{c1}\,\varepsilon\,\sigma\,T_{c1,i}^4 - h_{c1-g}\,A_{c1}\,(T_{c1,i} - T_{g,i}) = 0 \tag{6}$$

Equation 6 has to be solved for the unknown, $T_{c1,i}$. The term, $Q_{ab,c1,i}$ is obtained from MC ray tracing. The gas temperature $T_{g,i}$ is calculated by solving the energy equation for the gas phase as explained later. Once both absorption term and gas temperatures are treated as known quantities in equation (6), we have a fourth-order equation for $T_{c1,i}$ as shown below,

$$A\,T_{c1,i}^4 + B\,T_{c1,i} + C = 0 \tag{7}$$

where $A = -A_{c1}\,\varepsilon\,\sigma$, $B = -h_{c1-g}\,A_{c1}$ and $C = Q_{ab,c1,i} + h_{c1-g}\,A_{c1}T_{g,i}$

Following same procedure as for c_1, the cylindrical cavity c_2 is split into $M2$ isothermal ring elements of equal width $w_{c2}=L_2/M2$ with inner and outer radius of R_{2in} and R_{2out} respectively. Just as in case for c_1, neglecting axial conduction and assuming perfectly insulated outer surface, we can apply the steady state energy conservation for each ring element. For an element i of c_2, the absorbed energy ($Q_{ab,c2,i} = Q_{1,ab,c2,i} + Q_{2,ab,c2,i}$) is composed of contributions from incident solar radiation and emissions from other surface elements of the reactor. This energy is then either lost by convection to adjacent gas phase of air or re-radiated. We write steady state energy equation by applying an energy balance to a ring element i.

$$Q_{ab,c2,i} - Q_{em,c2,i} - Q_{conv,c2-g,i} = 0 \tag{8}$$

As derived for c_1, equation (8) can be re-written as a 4th order equation to be solved for $T_{c2,i}$,

$$P\,T_{c2,i}^4 + Q\,T_{c2,i} + R = 0 \tag{9}$$

where $P = -A_{c2}\,\varepsilon\,\sigma$, $Q = -h_{c2-g}\,A_{c2}$ and $R = Q_{ab,c2,i} + h_{c2-g}\,A_{c2}T_{g,i}$. The area $A_{c2} = 2\pi R_{2in}\ w_{c2}$. The heat transfer coefficient h_{c2-g} is calculated from Nu which is obtained using equation 4. It is then found in the same manner as h_{c1-g} was calculated.

For the front plate *(fp)*, back plate *(bp)* and connecting plate *(cp)*, the control volume elements are chosen as rings of thickness equal to t_{fp}, t_{cp}, and t_{bp} respectively. *fp* is split into $M3$ elements of width, $w_{fp}= (R_{fpout} -R_{ap})/M3$. Similarly *cp* and *bp* are also split into $M4$ and $M5$ elements, of widths $w_{cp}= (Rcp_{out} -Rcp_{in})/M4$ and $w_{bp}= (Rbp_{out} -R_{ex})/M5$ respectively. For each of these elements, at steady state, it is assumed that energy absorbed is only lost through emission. The losses due to convection to gas phase and conduction is assumed to be negligible. Hence we can write for an ith element,

$$Q_{ab,fp,i} - Q_{em,fp,i} = 0 \tag{10}$$
$$Q_{ab,cp,i} - Q_{em,cp,i} = 0 \tag{11}$$
$$Q_{ab,bp,i} - Q_{em,bp,i} = 0 \tag{12}$$

Again all absorption terms are obtained from MC ray tracing. The emission terms are calculated as follows

$$Q_{em,fp,i} = A_{fp,i}\varepsilon\,\sigma\,T_{fp,i}^4 \tag{13}$$
$$Q_{em,cp,i} = A_{cp,i}\varepsilon\,\sigma\,T_{cp,i}^4 \tag{14}$$
$$Q_{em,bp,i} = A_{bp,i}\varepsilon\,\sigma\,T_{bp,i}^4 \tag{15}$$

Here, $A_{fp,i} = \pi\,w_{fp}\,(2R_{ap} + w_{fp})$, $A_{cp,i} = \pi\,w_{cp}\,(2Rcp_{in} + w_{cp})$ and $A_{bp,i} = \pi\,w_{bp}\,(2Rbp_{in} + w_{bp})$. Temperatures for surface elements of *fp, cp* and *bp* are found by combining equations 10 through 12 and equations 13 through 15 as follows,

$$T_{fp,i} = \left(\frac{Q_{ab,fp,i}}{A_{fp,i}\varepsilon\,\sigma}\right)^{1/4} \tag{16}$$

$$T_{cp,i} = \left(\frac{Q_{ab,cp,i}}{A_{cp,i}\varepsilon\,\sigma}\right)^{1/4} \tag{17}$$

$$T_{bp,i} = \left(\frac{Q_{ab,fp,i}}{A_{bp,i}\varepsilon\,\sigma}\right)^{1/4} \tag{18}$$

For gas phase of air, fluid domain is split into isothermal disks of equal widths. For domain extending from $z=0$ to $z=L_1$ (inside cavity c_1) it is split into M6 isothermal disks of equal width, $w_{g1} = (L_1)/M6$ and radius, R_{1in}. Similarly, the fluid domain inside c_2 located between $z= L_1$ and $z=L_2$, is divided into M7 isothermal disks of equal width, $w_{g2} = (L_2)/M7$ and radius, R_{2in}. The choice of control volume in the form of disks

is made by keeping in mind that the motivation here is to obtain axial temperature distribution in the fluid. So, it is assumed that the gas enters the control volume with a uniform temperature, $T_{g,i}$ and exits with a temperature, $T_{g,i+1}$. As air is considered non-participating, it does not absorb or emit radiation. The enthalpy change of the gas (Δh_g) as it enters and leaves the control volume is solely due to convective heat transfer from the reactor walls. Figure 7 shows a representative control volume with all energy terms, for the gas medium inside c_1 and c_2.
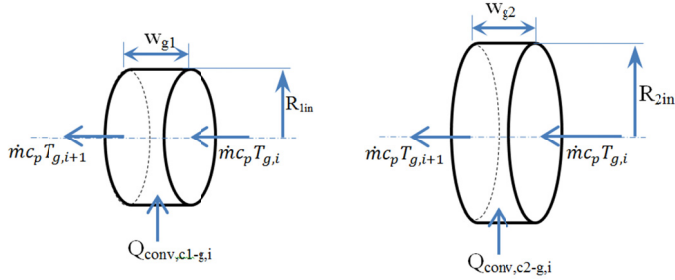
Figure 7 On the left is a control volume for air inside cavity c_1. On the right is the control volume for air inside cavity c_2. Incoming and outgoing energy are indicated for both.

A steady state energy balance for a control volume of air inside cavity c1 ($0 \leq z < L_1$), is given as,

$$Q_{conv,c1-g,i} - \dot{m}_g c_p (T_{g,i+1} - T_{g,i}) = 0 \qquad (19)$$

The convection term $Q_{conv,c1-g,i}$ is given by equation 3. Here c_p= 1189 J/kg.K and for all studies presented here, a volume flow rate of 10 l/min is used. This corresponds to a mass flow rate of $\dot{m}_g = 1.936 \times 10^{-4}$ kg/s.

Similarly, for a control volume inside cavity c_2 ($L_1 \leq z \leq L_2$),

$$Q_{conv,c2-g,i} - \dot{m}_g c_p (T_{g,i+1} - T_{g,i}) = 0 \qquad (20)$$

Knowing the inlet gas temperature, $T_{g,in}$ (Taken to be ambient temperature of 300K) at node $i=1$ $(z=0)$, we can calculate the temperature of gas at the next node, $i=2$. Using equations (19) and (20), we can find the gas temperature at each subsequent node up to $z=L_2$.

Equations (7), (9), (19) and (20) are a coupled system of equations to be solved for the unknowns, $T_{c1,i}$, $T_{c2,i}$ and $T_{g,i}$. $T_{fp,i}$, $T_{cp,i}$ and $T_{bp,i}$ are calculated from equations 16 through 18. The absorption terms are first obtained from MC ray tracing using a guess for initial temperature distribution. Then, using equations (7), (9), (16), (17), (18), (19) and (20), the new temperature distributions are found which is again used for the MC ray tracing to find the absorption terms. The iteration is continued between the energy equations and MC ray tracing until the overall energy balance for the system is satisfied as explained in the next section.

Monte Carlo Method
The Monte Carlo (MC) method refers to a group of numerical techniques that are based on calculation of statistical characteristics of physical processes that are deterministic. MC method is often employed to analyse complex problems whose behaviour is not predicted easily or accurately by direct experimental or analytical methods. The basis of any MC method is the use of randomly generated numbers as a means to calculate the expected outcome of any process that is by itself not random. So a MC method essentially replaces a physical process by a probabilistic model that simulates the actual behaviour, but is far easier to analyse, and is expected to produce the same outcome as the actual process [17].

MC Ray tracing
The MC ray tracing method uses a probabilistic model of radiative energy exchange to simulate radiative heat transfer in a system [17, 18]. The ray tracing method replaces the actual radiative exchange by a statistical method that captures behaviour of the total system as an average of frequency of events that have occurred. In a radiative heat exchange process with a non-participating medium, the events that occur can be broadly classified in to irradiation, absorption, emission and reflection. The incident solar radiation can be either absorbed or reflected by the cavity walls. The aim of MC ray tracing method is to obtain the net radiative flux for each element involved in the radiation exchange process. In ray tracing, total energy from all incident radiation is divided equally among a number of rays. Incident radiation includes primary rays from the incoming solar radiation and secondary rays due to emission from the cavity walls. Each ray is assigned a direction that has been generated such that it follows the probability density functions demanded by the actual physical process in hand. Then the ray is followed as it traverses through the medium. For each possible event, there is a probability density function that is associated with it. This decides which one of the events would occur based on a randomly generated number. Then, the ray is either absorbed or reflected at the walls. Each ray is followed until it is absorbed by the walls or lost from the system as re-radiation through the aperture or through the exit port of the reactor. The average behaviour of a large number of such rays provides the radiative performance of the receiver. In MC method, along the path of a ray, each event is considered independent of the preceding event.

The major advantage of MC ray tracing method is that it is not limited to treating diffuse-gray-isotropic problems. Most analytical techniques would require these assumptions and simple geometries. With MC ray tracing, one can treat non-diffuse, non-gray, non-isothermal and anisotropic problems with complex 3D geometries.

Here, the cavity walls are assumed to be diffuse-gray surfaces. In the gas phase, air is considered as a non-participating medium.

Step 1: Dividing solar radiation and emission from control volume elements into rays

The solar radiation intercepted at the aperture is assumed to have a Plank's black body spectral distribution [17] at 5780 K and is assumed to be uniformly distributed over the aperture. The total solar energy incident at the aperture is Q_{solar} ($=P_{ap}$). This energy is split equally between $N'_{S,rays}$ rays. This constitutes the primary rays. Each primary ray carries the energy,

$$Q_{prim} = Q_{solar}/N'_{S,rays} \quad (21)$$

Each subsystem element of the reactor also radiates energy by virtue of its temperature. This is designated as $Q_{em,c1,i}$, $Q_{em,c2,i}$, $Q_{em,fp,i}$, $Q_{em,bp,i}$ and $Q_{em,cp,i}$ for the cylindrical cavity wall elements of c_1 and c_2, front plate (*fp*), back plate (*bp*) and connecting plate (*cp*) for the ith element. Let emission from each element be split equally between $N'_{i,rays}$ rays. These are called secondary rays where energy of each ray is given by,

$$Q_{sec,c1,i} = Q_{em,c1,i}/N'_{i,rays} \quad (22)$$
$$Q_{sec,c2,i} = Q_{em,c2,i}/N'_{i,rays} \quad (23)$$
$$Q_{sec,fp,i} = Q_{em,fp,i}/N'_{i,rays} \quad (24)$$
$$Q_{sec,bp,i} = Q_{em,bp,i}/N'_{i,rays} \quad (25)$$
$$Q_{sec,cp,i} = Q_{em,cp,i}/N'_{i,rays} \quad (26)$$

For the very first iteration, we have assumed an initial temperature distribution equal to *500 K* for all surface to calculate $Q_{em,c1,i}$, $Q_{em,c2,i}$, $Q_{em,fp,i}$, $Q_{em,bp,i}$ and $Q_{em,cp,i}$ from

$$Q_{em,c1,i} = A_{c1}\, \varepsilon\, \sigma\, T^4_{c1,i} \quad (27)$$
$$Q_{em,c2,i} = A_{c2}\, \varepsilon\, \sigma\, T^4_{c2,i} \quad (28)$$
$$Q_{em,fp,i} = A_{fp,i}\varepsilon\, \sigma\, T^4_{fp,i} \quad (29)$$
$$Q_{em,bp,i} = A_{bp,i}\, \varepsilon\, \sigma\, T^4_{bp,i} \quad (30)$$
$$Q_{em,cp,i} = A_{cp,i}\, \varepsilon\, \sigma\, T^4_{cp,i} \quad (31)$$

Each of these rays (primary and secondary) is traced in the receiver until they are either absorbed by the surface elements or escapes through the aperture or exit of the reactor.

Step 2: Finding direction of primary/secondary rays
Ray tracing is a purely geometrical problem. It depends on determination of point of origin of the ray, the direction, and how it traverses through the medium. Here the gas medium is non-participating, so we only have to establish the location where the ray strikes the cavity walls. Once the location is found, the control volume corresponding to this location has to be determined.

Figure 8 shows the solar cavity-receiver positioned on axis with the solar concentrator [13] and aperture at the focal plane. The paraboloidal concentrator has a focal length, $f = 5\ m$ and radius $R_{conc} = 4.25\ m$. For initiating the Monte-Carlo technique of ray tracing, first we calculate the direction of the ray through the aperture and its point of origin on the aperture. This direction is

given by the unit vector $\hat{u} = \frac{P_2 - P_1}{|P_2 - P_1|}$ and P_2 is the point on the aperture from where the ray enters the receiver. P_1 and P_2 need to be found in order to obtain the direction of the ray into the aperture. Assuming uniform flux distribution, the number of rays from a certain ring of radius r is proportional to its normal projected area $2\pi r\, dr$. Let $N'_{S,rays}$ be the number of rays incident on the concentrator. Then,

$$N'_{S,rays} = C\, 2\pi r\, dr \quad for\ R_{2out} < r < R_{conc}$$
$$= 0 \qquad\qquad else\ where \quad (32)$$
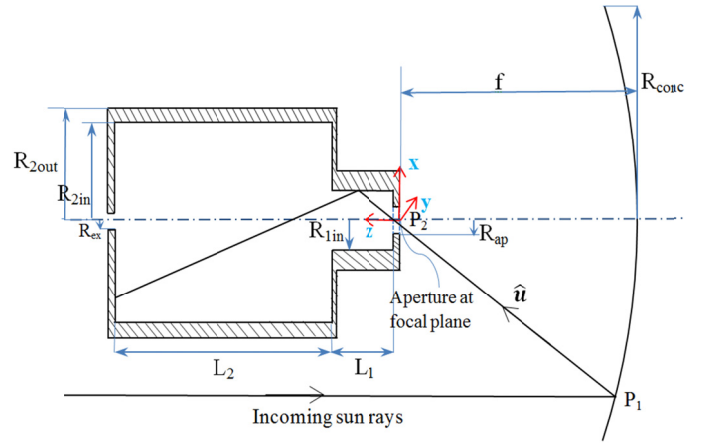
Figure 8 Scheme of solar reactor configuration with paraboloidal concentrator

The probability distribution for a ray hitting a particular radius r is given by

$$P(r) = \frac{C_1 r}{\int_{R_{2out}}^{R_{conc}} C_1 r\, dr} = \frac{2r}{R^2_{conc} - R^2_{2out}}\ for\ R_{2out} < r < R_{conc}$$
$$= \quad 0 \qquad\qquad else\ where \quad (33)$$

The cumulative distribution function is calculated by

$$R_1 = \int_{-\infty}^{r} P(r')dr' = \int_{R_{2out}}^{r} P(r')dr' \quad (34)$$
$$= \frac{r^2 - R^2_{2out}}{R^2_{conc} - R^2_{2out}}$$

Equation (34) can be rewritten as

$$r^2 = R_1(R^2_{conc} - R^2_{2out}) + R^2_{2out} \quad (35)$$

Likewise, we can find the polar angle, θ using

$$\theta = 2\pi R_2 \quad (36)$$

Here R_1 and R_2 are random numbers chosen from a uniformly distributed set between 0 and 1. These are generated by a pseudo-random number generator using a computer program and inserted into the equations (35) and (36) to get r and θ. Once these are calculated, the coordinates of P_1 are given as

$$P_1 = [r.\cos\theta, r.\sin\theta, -(f - \frac{r^2}{4f})] \tag{37}$$

Using the same approach we can assign two more random numbers, R_3 and R_4 to calculate the location of P_2 as shown below,

$$r = R_{ap}\sqrt{R_3} \tag{38}$$
$$\varphi = 2\pi R_4 \tag{39}$$
$$P_2 = [r.\cos\varphi, r.\sin\varphi, 0] \tag{40}$$

By using guesses for the random numbers, a random direction for the ray is obtained as $\hat{u} = \frac{P_2 - P_1}{|P_2 - P_1|}$. This ray enters the aperture at a random location, P_2.

After the direction of incoming radiation through the aperture $\hat{u}$ is calculated, we need to find out where it intersects the interior of the receiver. For that we define a line in the direction of $\hat{u}$ in parametric form as,

$$\vec{r_{ray}} = \vec{OP_2} + t\,\hat{u} \tag{41}$$

where t is a parameter which can be varied to generate the line and O is the origin of the co-ordinate system.

The inner surface of cylindrical cavity c_1 can be represented in parametric form as follows,

$$\vec{r_{c1}}(\theta, s) = R_{1in}\cos\theta\,\hat{i} + R_{1in}\sin\theta\,\hat{j} + s\,\hat{k} \tag{42}$$
$$for\ \ [0 \le \theta \le 2\pi]\ and\ [0 \le s \le L_1]$$

Here θ and s are the parameters that generate the inner surface of the cavity c_1.

Let $\vec{OP_2} = \vec{b} = b_1\,\hat{i} + b_2\,\hat{j} + b_3\,\hat{k}$ and $\hat{u} = u_1\,\hat{i} + u_2\,\hat{j} + u_3\,\hat{k}$.

We need to find the intersection of incoming ray with the cylinder surface. Equating equations (41) and (42), we get,

$$(b_1 + t\,u_1)\,\hat{i} + (b_2 + t\,u_2)\,\hat{j} + (b_3 + t\,u_3)\,\hat{k} \tag{43}$$
$$= R_{1in}\cos\theta\,\hat{i} + R_{1in}\sin\theta\,\hat{j} + s\,\hat{k}$$

Equating x, y and z components separately we get 3 equations that have to be solved for the unknowns t, θ and s.

$$(b_1 + t\,u_1) = R_{1in}\cos\theta \tag{44}$$
$$(b_2 + t\,u_2) = R_{1in}\sin\theta \tag{45}$$
$$(b_3 + t\,u_3) = s \tag{46}$$

Eliminating θ from equations (44) and (45) we get a quadratic equation for t,

$$At^2 + Bt + C = 0 \tag{47}$$

Here $A = u_1^2 + u_2^2$, $B = 2(b_1 u_1 + b_2 u_2)$ and $C = b_1^2 + b_2^2 - R_{1in}^2$

When $t \le 0$, the incoming ray does not intersect the cylinder.

The z – coordinate for intersection of line with cylindrical cavity c_2 is calculated from equation (46). If the calculated s is within the bounds indicated in equation (42) ($s \le L_1$), then the ray intersects the cylinder surface 1. The point of intersection is then obtained from equation (41) by substituting for the value of t from (47). However, if $s > L_1$ then we need to repeat a similar procedure as outlined above to check if the incoming ray intersects the inner surface of c_2.

To verify intersection of the incoming ray with c_2, we repeat above procedure for c_2 just as we did for c_1. Now s is re-calculated and if $L_1 < s < L_1 + L_2$, then incoming ray intersects with c_2. However, if $s \ge L_1 + L_2$ then, we check for possible intersection on the surface of the back plate.
The parametric form of surface of back plate is written as

$$\vec{r_{bp}}(\theta, R) = R\,\cos\theta\,\hat{i} + R\,\sin\theta\,\hat{j} + (L_1 + L_2)\,\hat{k} \tag{48}$$
$$for\ [0 \le \theta \le 2\pi]\ and\ [0 \le R \le R_{2in}]$$

In order to determine the point of intersection we have to equate equations (41) and (48).

$$(b_1 + t\,u_1) = R\,\cos\theta \tag{49}$$
$$(b_2 + t\,u_2) = R\,\sin\theta \tag{50}$$
$$(b_3 + t\,u_3) = (L_1 + L_2) \tag{51}$$

From equation 51, we can calculate parameter t. Then, equation (43) gives the co-ordinates of point of intersection of the ray with back plate. The radius R at which intersection takes place is calculated by combining equations (49) and (50),

$$R = \sqrt{(b_1 + t\,u_1)^2 + (b_2 + t\,u_2)^2} \tag{52}$$

If $R < R_{ex}$, then the ray escapes the receiver through the exit. The history of this ray is terminated and recorded as energy lost. Now go to step 4 to check if all primary rays have been traced.

In case of intersection with c_1, c_2 or bp go to step 3 to verify whether reflection or absorption takes place at the surface.

Secondary ray emission from walls
Simultaneously, there are secondary rays emanating from the cavity walls. Trace a ray each from the control volume element, i.

When energy is absorbed by the receiver walls, at steady state, it is either lost through convection to gas phase or lost through re-radiation. The emitted energy from the wall elements are given by equations (27) through (31). Here again we need to find the direction of the secondary ray. Assuming diffuse-gray

properties for the walls, we can calculate the polar and cone angles by defining the random numbers R_{14} and R_{15} as,

$$\theta = \sin^{-1}\sqrt{R_{14}} \tag{53}$$
$$\varphi = 2\pi R_{15} \tag{54}$$

Step 3: Absorption or Reflection from walls
If a ray primary or secondary reaches a wall element, we need to check if absorption or reflection occurs. It is decided by generating another random number, R_{11}. The criterion is as follows

Case I absorption when : $R_{11} \leq \alpha$ (55)

Case II reflection occurs when : $R_{11} > \alpha$ (56)

Here $\alpha = \varepsilon = 0.8$ by Kirchoff's law for diffuse-gray surfaces [17]. If Case I occurs, the ray is absorbed and recorded by counters. If it is a primary ray that is absorbed then the counter $n_{p,ab,c1,i}$, $n_{p,ab,c2,i}$, $n_{p,ab,fp,i}$, $n_{p,ab,bp,i}$ or $n_{p,ab,cp,i}$ is incremented depending on where the ray is absorbed and its history is terminated. If it is a secondary ray, depending on the source of the ray the counters, $n_{sec,ab,c1,i-c1,j}$, $n_{sec,ab,c1,i-c2,j}$, $n_{sec,ab,c1,i-fp,j}$ and $n_{sec,ab,c1,i-bp,j}$ are incremented for absorption by c_1. For absorption by c_2 we have the counters, $n_{sec,ab,c2,i-c1,j}$, $n_{sec,ab,c2,i-c2,j}$, $n_{sec,ab,c2,i-cp,j}$, $n_{sec,ab,c2,i-fp,j}$ and $n_{sec,ab,c2,i-bp,j}$. The back plate sees all other surfaces (does not see itself). So for absorption by bp, we have to increment the counters, $n_{sec,ab,bp,i-c1,j}$, $n_{sec,ab,bp,i-c2,j}$, $n_{sec,ab,bp,i-cp,j}$, and $n_{sec,bp,c2,i-fp,j}$. The connecting surface, cp sees elements on surfaces of bp and c_2. So for absorption by connecting plate cp the counters $n_{sec,ab,cp,i-bp,j}$ and $n_{sec,ab,cp,i-c2,j}$ are incremented. The surface, fp sees all surfaces of the receiver other than cp and itself. Any absorption by elements of fp are recorded by incrementing the counters, $n_{sec,ab,fp,i-c2,j}$, $n_{sec,ab,fp,i-c1,j}$ and $n_{sec,ab,fp,i-bp,j}$. Go to step 4.

If case II occurs, diffuse-gray reflection is assumed from the surface. The wavelength of the reflected ray remains unchanged. The direction of the reflected ray is calculated by generating two random numbers, R_{12} and R_{13} to calculate the polar and cone angles:

$$\theta = \sin^{-1}\sqrt{R_{12}} \tag{57}$$
$$\varphi = 2\pi R_{13} \tag{58}$$

The reflected ray is then traced to find location of its intersection with the walls in a similar manner as outlined in step 2. If it escapes through the exit or aperture its history is terminated and go to step 4. Otherwise, if an intersection occurs with the surface elements of the wall, then go to step 3 to ascertain if absorption or reflection takes placed. This process is continued until the ray is either absorbed or escapes the receiver.

Step 4: Check number of primary and secondary rays emitted

If all primary rays $N'_{S,rays}$ and secondary rays $N'_{i,rays}$ have been traced, then go to step 5. Otherwise, go back to step 2.

Step 5: End of iteration: Calculation of absorption terms
One iteration of Monte Carlo ends by the calculation of the absorption terms. The absorption terms for a c_1 wall volume element, i are calculated as:

$$Q_{ab,c1,i} = Q_{1,ab,c1,i} + Q_{2,ab,c1,i} \tag{59}$$
$$= n_{p,ab,c1,i} \cdot Q_{prim} +$$
$$\sum_{j=1}^{M1} n_{sec,c1,i-c1,j} \cdot Q_{sec,c1,j} + \sum_{j=1}^{M5} n_{sec,ab,c1,i-bp,j} \cdot Q_{sec,}$$
$$+ \sum_{j=1}^{M2} n_{sec,ab,c1,i-c2,j} \cdot Q_{sec,c2,j} +$$
$$\sum_{j=1}^{M3} n_{sec,ab,c1,i-fp,j} \cdot Q_{sec,fp,j}$$

Similarly for back plate

$$Q_{ab,bp,i} = Q_{1,ab,bp,i} + Q_{2,ab,bp,i} \tag{60}$$
$$= n_{p,ab,bp,i} \cdot Q_{prim} + \sum_{j=1}^{M2} n_{sec,ab,bp,i-c2,j} \cdot Q_{sec,c2,j} +$$
$$\sum_{j=1}^{M1} n_{sec,ab,bp,i-c1,j} \cdot Q_{sec,c1,j} +$$
$$\sum_{j=1}^{M4} n_{sec,ab,bp,i-cp,j} \cdot Q_{sec,cp,j} +$$
$$\sum_{j=1}^{M3} n_{sec,ab,bp,i-fp,j} \cdot Q_{sec,fp,j}$$

For cylindrical cavity c_2

$$Q_{ab,c2,i} = Q_{1,ab,c2,i} + Q_{2,ab,c2,i} \tag{61}$$
$$= n_{p,ab,c2,i} \cdot Q_{prim} + \sum_{j=1}^{M5} n_{sec,ab,c2,i-bp,j} \cdot Q_{sec,bp,j} +$$
$$\sum_{j=1}^{M4} n_{sec,ab,c2,i-cp,j} \cdot Q_{sec,cp,j} +$$
$$\sum_{j=1}^{M2} n_{sec,ab,c2,i-c2,j} \cdot Q_{sec,c2,j} +$$
$$\sum_{j=1}^{M1} (n_{sec,ab,c2,i-c1,j} \cdot Q_{sec,c1,j} +$$
$$n_{sec,ab,c2,i-c1,j} \cdot Q_{sec,c1,j})$$

Likewise, for connecting plate, cp:

$$Q_{ab,cp,i} = Q_{1,ab,cp,i} + Q_{2,ab,cp,i} \tag{62}$$
$$= n_{p,ab,cp,i} \cdot Q_{prim} + \sum_{j=1}^{M5} n_{sec,ab,cp,i-bp,j} \cdot Q_{sec,bp,j} +$$
$$\sum_{j=1}^{M2} n_{sec,ab,cp,i-c2,j} \cdot Q_{sec,c2,j}$$

For the front plate, fp,

$$Q_{ab,fp,i} = Q_{1,ab,fp,i} + Q_{2,ab,fp,i} \tag{63}$$
$$= n_{p,ab,fp,i} \cdot Q_{prim} + \sum_{j=1}^{M5} n_{sec,ab,fp,i-bp,j} \cdot Q_{sec,bp,j} +$$
$$\sum_{j=1}^{M2} n_{sec,ab,fp,i-c2,j} \cdot Q_{sec,c2,j} +$$
$$\sum_{j=1}^{M1} n_{sec,ab,fp,i-c1,j} \cdot Q_{sec,c1,j}$$

The Monte Carlo routine ends here, go to Step 6

**Step 6: Numerical Solution of Governing Equations**
Once the absorption terms are available from step 5, the energy conservation equations 7, 9, 16, 17, 18, 19 and 20 can be solved to obtain $T_{c1,i}^n$, $T_{c2,i}^n$, $T_{fp,i}^n$, $T_{cp,i}^n$ and $T_{bp,i}^n$ where superscript indicates the iteration number. These temperatures are then provided to the MC ray tracing module to calculate the absorption terms again. The absorption terms are then

transferred to the energy solver to calculate the new temperature distribution $T_{c1,i}^{n+1}$, $T_{c2,i}^{n+1}$, $T_{fp,i}^{n+1}$, $T_{cp,i}^{n+1}$ and $T_{bp,i}^{n+1}$. This process of iterating between the MC ray tracing module and energy solver is continued until the overall energy balance for the whole system is satisfied, $|Q_{solar} - Q_{re-radiation} - Q_{convection}| < 10^{-5}$.

VALIDATION OF NUMERICAL METHOD

As a first step, the MC ray tracing code is validated by comparing our results for apparent absorptivity with those provided in [22]. In [22] the receiver has a simpler geometry consisting of a single cylindrical cavity with a back wall and a front wall that has the aperture.
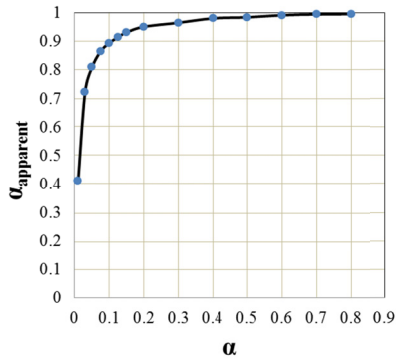
Figure 9 Variation of apparent absorptivity of the receiver plotted as a function of surface absorptivity

To draw a comparison, we simplified our domain so that it has exactly the same dimensions of the reactor in [22]. This is done by setting $L_1 = 0$, $R_{ap}=20mm$, $R_{2in} =55$ mm, $R_{2out}=150mm$ $L_2=0.263m$ and $P_{ap}=4kW$. Figure 9 shows the apparent absorptivity of the receiver as a function of surface absorptivity we have obtained using our code. Apparent absorptivity, $\alpha_{apparent}$ is calculated using MC ray tracing by counting the number of absorptions by inner surface of the cavity. It is the ratio of the number of rays absorbed by the receiver walls to the number of primary rays entering the reactor. The cavity absorbs the incident solar radiation directly or after multiple reflections. Here, $\alpha_{apparent}$ is calculated as surface absorptivity α is varied from *0.01* to *0.8*. The results obtained are in excellent agreement with Figure 2 of [22] for radius of aperture equal to *20 mm*. This provides a validation of the MC ray tracing part of the code.

As a second step of validation, for the same geometry, we calculated the stagnation temperature distribution after coupling the energy solver with the validated MC ray tracing module. Stagnation temperature is defined as the highest possible temperature that the receiver would attain at equilibrium in the absence of energy losses, for example by convection or conduction. There are no conduction losses due to assumption of perfect insulation of receiver walls. To neglect convection losses h_{c1-g} and h_{c2-g} are set to zero. The energy equations are then solved in conjunction with the MC ray tracing module until an overall energy balance is obtained as explained in step

6 of previous section. For MC ray tracing, we used *600,000* primary rays ($N'_{S,rays}$) and a total of *1,500,000* secondary rays. Figure 10 shows stagnation temperature distribution of receiver wall for an incoming solar power input Q_{solar} of *4kW*. In [22] the axial distances were measured from the back plate, as the origin of the co-ordinate system used was located on the back plate. However, in the present work, the co-ordinate system is located in the focal plane as shown in the schematic of Figure 5. To enable a back to back comparison with [22], in Figure 10, we have shown the variation of stagnation temperature with z*, where z* is the distance measured from the back plate. Again an excellent agreement is obtained with results given in [22].
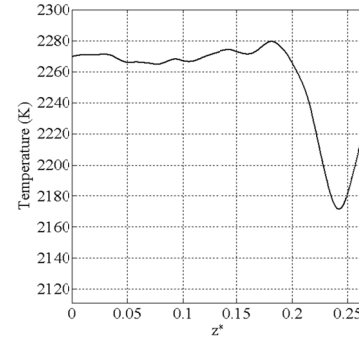
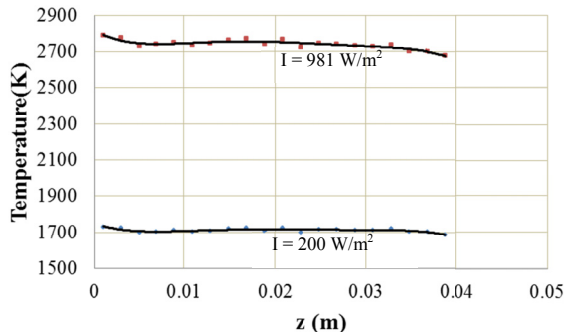**Figure 10** Stagnation temperature distribution for receiver walls along z*-direction

RESULTS

Figures 11 and 12 show temperature distribution of the cavity walls c_2 and c_1 corresponding to a normal insolation of 200 W/m^2 (corresponding to 0449 hrs and 1921 hrs) and peak insolation of 981 W/m^2 (at 1231 hrs) when the diameter of aperture is fixed at 4 cm. For this aperture size, the power intercepted by the aperture ($Q_{solar} = P_{ap}$) is 1.11 kW and 5.49 kW for normal insolation of 200 W/m^2 and 981 W/m^2 respectively (see figure 4). Out of 1.11 kW of power that is intercepted by the aperture in the morning or evening, 0.71 kW is re-radiated. This corresponds to about 64% of the incoming power lost through the aperture. A small amount, corresponding to about 4% is lost as radiation through exit port of the receiver. The rest 32 % is transferred by convection from the walls to the gas resulting in rise in gas temperature.
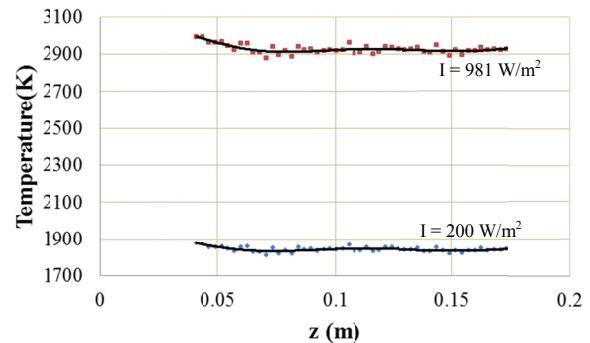
Figure 11 Temperature distribution of cavity walls c_2 corresponding to normal insolation of 200 W/m^2 and 981 W/m^2

For peak insolation, 84 % of the intercepted energy is re-radiated, 5 % is lost through exit port and 11% is transferred to the gas. From figures 11 and 12 it is clearly evident that the temperature distribution for the cavity walls remains nearly constant in the z-direction. For peak insolation, the cavity walls attain an average temperature of about 2800K, whereas at low insolation of 200 W/m^2, the average temperature is about 1800K.

Figure 12 Temperature distribution of cavity walls c_1 corresponding to normal insolation of 200 W/m^2 and 981 W/m^2

Figure 13 illustrates the variation of gas temperature inside the cavity. The gas enters the cavity at ambient temperature of 300 K. The cavity walls absorb the incoming solar radiation and transfer the energy to the gas via convection, thus heating the gas. For insolation of 200 W/m^2, the gas attains a constant temperature of about 1815K for $z > 0.1\ m$. Similarly for higher insolation of 981 W/ m^2, the gas attains a constant temperature of about 2900 K for $z > 0.05\ m$.
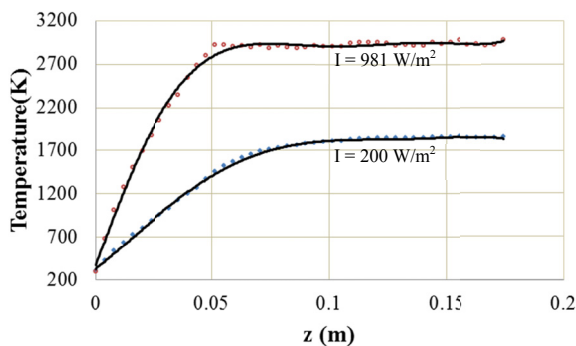

Figure 13 Gas temperature variation inside the cavity corresponding to normal insolation of 200 W/m^2 and 981 W/m^2

To study the effect of variable aperture size on the average gas temperature inside the reactor we performed the heat transfer and optical analysis for five levels of direct normal insolation 200 W/m^2, 400 W/m^2, 600 W/m^2, 800 W/m^2 and 981 W/m^2 available at different times of the day as indicated in Figure 3.

For each insolation level, the effect of employing apertures of different sizes ranging from minimum diameter of 1 cm to a maximum of 8 cm is investigated. Figure 14 depicts the variation of average gas temperature in the reactor when the

aperture diameter is changed for each level of insolation. As the aperture diameter is increased the average gas temperature keeps increasing until it reaches a maximum for an optimum diameter. Beyond this optimum value, although the power intercepted by the aperture is higher the re-radiation losses are also higher. Therefore, it is evident that there is an optimum aperture size beyond which the temperature in the reactor would start to drop.
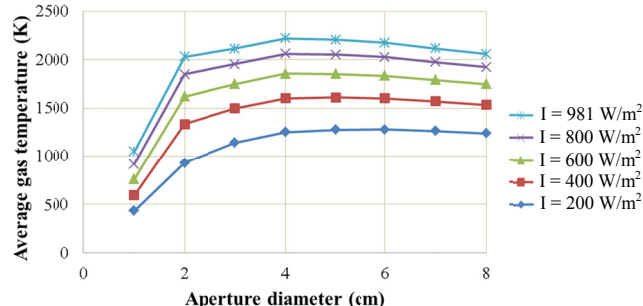
Figure 14 Average gas temperature plotted as a function of aperture diameter for different levels of normal insolation.

For instance at 0512 hrs or 1858 hrs, when the normal insolation is 400 W/m^2, the maximum average gas temperature of 1611K is obtained for an aperture diameter of 5 cm. For this aperture size, the incoming solar power input is 3.26 kW. Out of this, 2.68 kW escapes as re-radiation through the aperture. A small amount equal to 0.11 kW escapes through the exit port. The remaining 0.47 kW which is only about 14% of the power intercepted at the aperture is transferred to the gas from the wall. Now, for the same level of insolation, when the aperture diameter is increased to 8 cm, the power intercepted is much higher at about 6.13 kW. Compared to 5 cm opening, an aperture diameter opening of 8 cm lets in almost double the energy. However, it is observed that the larger opening leads to higher re-radiation losses of about 5.56 kW. Only about 7% of the incoming energy is transferred to the gas. This leads to a drop in temperature to 1533 K as shown in Figure 14.

For normal solar reactor operation, it is desirable to maintain the gas temperature semi-constant with respect to time. For example, solar thermal cracking of methane requires a temperature of 1500 K inside the reactor [19]. In order to provide the necessary process heat at this temperature, the aperture size has to be changed depending on the changing normal insolation from the sun. It is clear from figure 14 that for attaining 1500K, the reactor would have to be started when the normal insolation is at least 400 W/m^2. For the normal insolation data used in this study, this corresponds to 0512 hrs in the morning. To obtain an average gas temperature of 1500K, the aperture diameter is 3 cm. When the normal insolation increases to 600 W/m^2 at 0544 hrs, the aperture has to be closed to get a diameter of 1.86 cm. Similarly the aperture would have to be further closed as the normal insolation increases until it hits the peak at about 1231 hrs. Here an aperture diameter of 1.5 cm would be sufficient to generate the required temperature. Further as the insolation reduces as the day progresses, the aperture would have to be opened and at

1858 hrs when the insolation is 400 W/m² the diameter should be back at 3 cm. As the insolation decreases further in the evening, opening the aperture will not provide us with the required temperature inside the reactor.

This method of changing aperture size to compensate for fluctuating solar energy is reminiscent of the human eye, wherein the pupils dilate to let in more light in dim settings while they shrink to block the light in bright conditions.

CONCLUSIONS

The heat transfer and optical analysis of the prototype reactor is done with a well validated MC ray tracing code coupled to a steady state energy solver. We have shown that for a fixed mass flow rate of the working fluid, it is possible to maintain a constant gas temperature in the reactor by varying the aperture size that mimics the human eye. In the example we considered, to obtain an average gas temperature of 1500K, we would have to operate the reactor between 0512 hrs in the morning and 1858 hrs in the evening when normal insolation is at least *400 W/m²*. At this level of insolation, an aperture diameter of *3 cm* is required. For peak insolation of *981 W/m²* which occurs at noon, an aperture diameter of *1.5 cm* would be sufficient.

The analysis presented here assumes a perfectly insulated reactor. Ideally we want the reactor to be perfectly insulated so that maximum amount of energy absorbed by the receiver walls is transferred to the gas. However, in reality usage of any insulation material would still result in losses to the outside environment from the reactor walls. This is the reason why the aperture diameters calculated here would be smaller compared to what would actually be required in practice. However, the objective of the present work is to show how semi-constant gas temperature inside a reactor could be maintained by use of variable size apertures. Even when conduction losses, losses by convection to the atmosphere or heat of reaction for thermochemical processing are included, the trends we have presented here are to be expected.

ACKNOWLEDGEMENT

REFERENCES

[1] Goswami D.Y., Kreith F., and Kreider J. F., Principles of solar engineering, *Taylor and Francis, 2nd edition,* 2000

[2] Pitz-Paal R., Botero NB., and Steinfeld A., Heliostat field layout optimization for high-temperature solar thermochemical processing, *Solar Energy*, vol. 85, 2011, pp. 334-343

[3] Haueter P., Moeller S., Palumbo R., and Steinfeld A., The production of zinc by thermal dissociation of zinc oxide— solar chemical reactor design, *Solar Energy*, vol. 67, 1999, pp. 161–167

[4] Steinfeld A., Brack M., Meier A., Weindenkaff A., and Wuillemin D., A solar chemical reactor for co-production of zinc and synthetic gas, *Energy*, vol. 23(10), 1998, pp. 803–814

[5] Berman A., Karn R. K., and Epstein M., A New Catalyst System for High-Temperature Solar Reforming of Methane, *Energy Fuels*, vol. 20, 2006, pp. 455-462

[6] Ozalp N., and Shilapuram V., Step-by-step methodology of developing a solar reactor for emission-free generation of hydrogen, *International Journal of Hydrogen Energy*, vol. 35, 2010, pp. 4484-4495

[7] Hirsch D., and Steinfeld A., Solar hydrogen production by thermal decomposition of natural gas using a vortex-flow reactor*, International Journal of Hydrogen Energy*, vol. 29 (1), 2004, pp. 47–55

[8] Abanades S., and Flamant G., Thermochemical hydrogen production from a two-step solar-driven water-splitting cycle based on cerium oxides, *Solar Energy*, vol. 80, 2006, pp. 1611–1623

[9] Dahl J. K., Buechler K. J., Weimer A. W., Lewandowski A., and Bingham C., Solar-thermal dissociation of methane in a fluid-wall aerosol flow reactor, *International Journal of Hydrogen Energy,* vol. 29, 2004, pp. 725-736

[10] Abanades S., and Flamant G., Production of hydrogen by thermal methane splitting in a nozzle-type laboratory-scale solar reactor, *International Journal of Hydrogen Energy*, vol. 30, 2005, pp. 843-853

[11] Kogan A., and Kogan M., The Tornado flow configuration - an effective method for screening of a solar reactor window, *ASME J Sol Energy Eng*, vol. 124, 2002, pp. 206-14

[12] Muradov N., Hydrogen via methane decomposition: an application for decarbonization of fossil fuels, *International Journal of Hydrogen Energy*, vol. 26, 2001, pp. 1165-1175

[13] Haueter P., Seitz T., and Steinfeld A., A new high-flux solar furnace for high-temperature thermochemical research, *Journal of Solar Energy Engineering,* vol. 121, 1999, pp. 77–80

[14] Retrieved from *NREL database* on April 10, 2012 at "http://www.nrel.gov/midc/srrl_rsp2"

[15] Bird R. E., and Hulstrom R. L., Simplified Clear Sky Model for Direct and Diffuse Insolation on Horizontal Surfaces, *Technical Report No. SERI/TR-642-761, Golden, CO: Solar Energy Research Institute*, 1981

[16] Steinfeld A., and Schubnell M., Optimum aperture size and operating temperature of a solar cavity-receiver, *Solar Energy*, vol. 50, 1993, pp.19–25

[17] Howell J.R., Siegel R., and Menguc M.P., Thermal Radiation Heat Transfer, 5th Edition. *CRC Press, New York*, 2011

[18] Howell J. R., The Monte Carlo Method in Radiative Heat Transfer, *Journal of Heat Transfer,* vol. 120, 1998, pp. 547-560

[19] Hirsch D., and Steinfeld A., Radiative transfer in a solar chemical reactor for the co-production of hydrogen and carbon by thermal decomposition of methane, *Chem Eng Sci*, vol. 59, 2004, pp. 5771–5778

[20] Szekely J., and Carr R., Heat transfer in a cyclone, *Chemical Engineering Science*, vol. 21, 1966, pp. 1119–1132

[21] Ozalp N., and Kanjirakat A., Lagrangian characterization of multi-phase turbulent flow in a solar reactor for particle deposition prediction, *International Journal of Hydrogen Energy*, Vol. 35, 2010, pp. 4496-4507

[22] Kräupl S., Steinfeld A., Monte Carlo radiative transfer modeling of a solar chemical reactor for the co-production of Zinc and Syngas, *Journal of Solar Energy Engineering*, Vol. 127, 2005, pp. 102-108